Vehicular Communications 36 (2022) 100493

Contents lists available at ScienceDirect

Vehicular Communications

www.elsevier.com/locate/vehcom

Orientation of a diffuse reflector for improved coverage in ID-FSOC for vehicular communications

Paa Kwesi Esubonteng, Roberto Rojas-Cessa

Networking Research Laboratory, Department of Electrical and Computer Engineering, New Jersey Institute of Technology, Newark, NJ 07102, USA

ARTICLE INFO

Article history:
Received 14 October 2021
Received in revised form 2 March 2022
Accepted 31 May 2022
Available online 13 June 2022

Keywords:
Free-space optical communications
Optical wireless communications
Indirect optical communications
Diffuse reflection
Lambertian diffusion
Near optimal positioning of the diffuse reflector

ABSTRACT

Even with no line-of-sight (LoS), stations can optically communicate using Indirect line-of-sight diffused-light free-space optical communications (ID-FSOC). A diffuse reflector in the LoS of the stations reflects diffused light to them. But despite having diffused reflections in almost all directions, the orientation of a flat diffuse reflector defines the communications coverage. Therefore, there is a need for a tool that describes the relationship between the orientation of the diffuse reflector, the coverage, and the achievable data rates for the effective deployment of ID-FSOC. In this paper, we propose a model of the coverage of a diffuse reflector that can allow us to estimate the achievable data rates as a product of the orientation of the diffuse reflector. We use ground-to-vehicle communications as a demanding example scenario. We also propose RISE, a heuristic algorithm that optimizes the horizontal and vertical tilt angles of the reflector to maximize the achievable data rates. We show that 50% or more of the transmitted power of light is reflected, thereby achieving 1 Gbps or higher data rates across the optical local area network.

1. Introduction

Free-space optical communications (FSOC), also known as optical wireless (OW), can achieve higher data rates than radio frequency (RF) communication systems [1–3]. Its many desirable features, including long-distance communication range [4–6], high data rates, eavesdrop proof [7,8], and immunity to electromagnetic interference [9] make FSOC an attractive wireless communications technology for a wide range of application scenarios. Some of its applications are found in deep space, terrestrial, underwater, and inter-satellite communications [7,10].

But despite its very-high data rate capability as a wireless technology, FSOC adoption is lacking and behind RF technologies in a large measure. Major culprits on its limited adoption are the required direct line-of-sight (LoS) between a transmitter and a receiver [11,12], the point-to-point optical communications link that must be established for data transmission caused by the inability of FSOC to operate with multiple access as its RF counterpart does, where multiple stations can directly communicate with others. However, we argue that such a limitation is not caused by the light but how it is handled.

Indirect LoS with diffused light FSOC, or ID-FSOC, is a more robust approach than FSOC. It uses diffuse reflectors (DRs) to set up a communication link between a transmitter and a receiver [13–16]. ID-FSOC not only removes many of the limitations of FSOC but also unearths new properties without sacrificing its achievable data rates under well defined conditions. As a DR, an ideal Lambertian surface reflects the transmitted light with an equal intensity in all directions except towards itself. Such DRs can be made from common materials, such as aluminum foil, polytetrafluoroethylene (PTFE) tape, and titanium dioxide paint. These materials can reflect close to 100% of transmitted light [17,18].

In ID-FSOC, a station projects a laser beam on the DR to transmit data and focuses its receiver on a DR to receive data. To a transmitting station, the DR is the intended receiver. Conversely, the DR is a transmitting source to a receiving station. ID-FSOC stations use an acquisition, tracking, and pointing (ATP) mechanism to point their transceivers to a DR, but unlike FSOC, the required alignment accuracy of an ATP in ID-FSOC is more relaxed because the DR size is larger than receiver lenses in FSOC. Different from FSOC, a transmission in ID-FSOC is detectable by all receivers who have LoS to the DR, just as a broadcast medium in what is naturally an optical local area network (OLAN). The high-speed channels of ID-FSOC can be further multiplied by using spatial diversity, where not one but multiple beams are projected on the DR at once.

E-mail addresses: pae5@njit.edu (P.K. Esubonteng), rojas@njit.edu (R. Rojas-Cessa).

https://doi.org/10.1016/j.vehcom.2022.100493
2214-2096/

Despite the highly uniform diffuse reflectance of a DR, the coverage is not equal on the whole covered area. The coverage is affected by the distance of the receiver from the DR, the angle of incident of a transmitted beam, and the orientation of the DR. Such orientation can be simply expressed as the horizontal and vertical tilt of the DR for a stationary one. These parameters must be considered in the deployment of ID-FSOC and optimized for a given scenario.

The search of an optimized coverage of the DR raises the following question: What is the position of the DR that would maximize the power reflected to stations for incident beams emitted from different incident angles? To answer this question, we propose a model to estimate an ID-FSOC network coverage as a function of the angle of incidence of a transmitted laser beam and the orientation of the DR. To make use of such model, we also propose a heuristic algorithm that determines the near optimal tilt of a diffuse reflector, or RISE for short. The model and RISE are a tool for determining the orientation of a DR in the deployment of ID-FSOC. Such a deployment mostly comprises the placement of a stationary optical base station (OBS) and a DR for each OLAN segment. We apply the model on a scenario of vehicular communications that uses an OBS for Internet access and cars as mobile stations.

The contributions of this work are three-fold: 1) We propose a model to compute the angle of incidence between the DR and a transmitter and the horizontal and vertical tilt angles of a DR for a given coverage, 2) we propose RISE, a heuristic algorithm that computes the near optimal tilt angles of the DR to provide the largest coverage for the mobile stations across the network, and 3) we show the relationship between the reflected power and the received power under different variation of design parameters and determine the achievable communication data rates.

The remainder of this paper is organized as follows. Section 2 describes related works. Section 3 introduces the proposed ID-FSOC framework and presents the analysis of the angle of incidence. Section 4 introduces our heuristic algorithm that computes the near optimal tilt of the DR that maximizes the covered area. Section 5 presents the achievable data rates through numerical evaluations. Section 6 draws our conclusions.

2. Related works

The use of reflected transmissions to improve and extend communication in networks has been addressed in both optical networks [16] and radio communications [19,20]. Masterson et al. [19] and Arun et al. [20] have suggested beamforming from reflected radiowaves as a technique to improve network throughput. This technique can extend the range of the network and increase data rates in communications. These works discuss installing reflective surfaces in parts of the network to reflect some of the energy from radiowaves towards specific regions with no line-of-sight or where coverage is minimal or non-existent. Here the reflective surface is a rectangular array of simple RF switch elements in either On and Off states, where the surface reflects RF transmissions when the switch is in the On state; or passes the signal through, if otherwise.

Diffused reflective screens enable simultaneous optical communications for multiple mobile stations without the use of multi-array LEDs directed towards multiple mobile stations in a network [21,22]. This arrangement reduces the amount of hardware required in an optical local area network (OLAN) by minimizing the number of optical transceivers (OTs) that an OBS uses to communicate with the mobile stations. ID-FSOC also promotes the development of standardized medium access control (MAC) schemes, permits the use of a shared backhaul, and provides larger margins for ATP alignment used by communicating stations. In a few words, an OLAN may simplify network management. Such OLANs also may support structured and ad-hoc communications among stations in the network.

Several works have targeted modeling and analysis of indoor optical networks using an indirect LoS technique [13,23,14], while others model the path of light rays in an indoor environment where an infra-red light is used to transmit data. The transmitter's modulated light is focused on the walls of a room, and an optical receiver detects the reflections from the wall [23,14]. Wu et al. [14] showed that in a rectangular shaped room, an elliptical shaped beam experiences a smaller decrease in power distribution than a circular shaped beam with the same divergence angle. Such gain would improve the received power of an indoor optical network.

The use of FSOC to exchange information between vehicles on a roadway has been studied in [24–29]. These works show achievable data rates between 0.5-40 Gbps for point-to-point optical links in a vehicular network using visible light. Here, an LED transmitter and a camera receiver are installed in a vehicle's headlight and taillight, respectively, such that the vehicle transmits using the LED light and receives a transmission using the camera receiver. Several works have shown feasibility of direct LoS vehicle-to-vehicle (V2V) optical communications in a noisy environment (e.g., rain, fog, and sunlight) [24,28–30].

Wilkins et al. [31] extended V2V communications infrastructure to fixtures (i.e., signposts, street lights, and traffic lights) of the moving vehicle's surrounding environments. In this setup, the OT is attached to fixtures to support bi-directional LoS communication between the fixtures and the vehicle. DRs in an optical network have been considered to provide outdoor bi-directional communications between an OBS and a vehicle [16,32]. The framework used by Kaymak et al. [16] established an uplink and downlink communication link by placing DRs in the sight of the OT of the moving vehicles and OBS. Results show achievable data rates of 0.3-1 Gbps. The configurations used compare the performance of the network when the DR is placed in front of a vehicle and on its side. Macaluso et al. [32] proposed the first MAC schemes for ID-FSOC that uses a DR to facilitate optical communication between mobile station and an OBS. This work showed space-time trade-offs may be considered in such access schemes.

DRs passively broadcast optical transmissions through the diffuse reflection of the incident light over their covered area. The reflected light allows multiple users to share an OBS. While FSOC requires a strict ATP alignment to compensate for slight shifts in alignment between communicating OTs that may result in a communication failure, the surface of the DR is relatively large so that it may prevent such a failure from happening under a similar slight alignment shift between the OTs and the DR. Also, a diffuse reflection relaxes ATP specifications for optical communication. The broadcast nature of the optical reflections serves multiple mobile stations located at different places of the covered area and also supports continuous communications as users move around the covered area. A DR can be easily installed to existing road fixtures with minimum infrastructural cost.

An important issue with ID-FSOC is the achievable data rates provided to the different locations within the area covered by the DR and the effect that the angle of incidence has on the power of the reflected beam. Here we focus on the relationship between the location of the mobile stations in the network and the angle of incidence of a transmission to the surface of the DR. This angle determines the amount of the reflected power on the covered space. The reflected power across the network is used in establishing the minimum reflected power, which in turn determines the received power and its corresponding data rate across the network. Furthermore, the data rate distribution determines the network size, the distance between DRs, and the placement of the OBS in the area

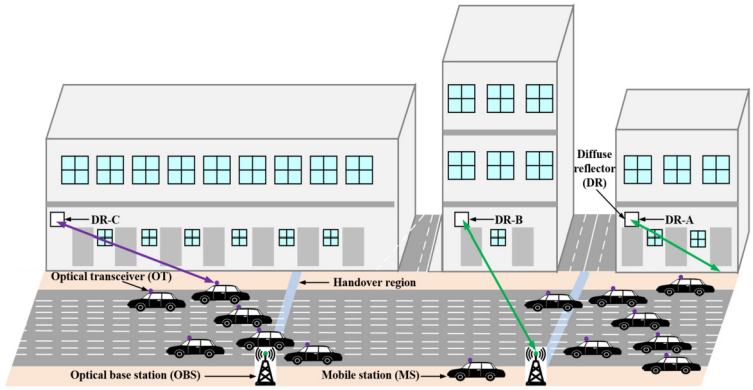

Fig. 1. Proposed optical local area network.

covered by the DR. Key factors to consider in an OLAN design using a DR are the desired size of covered area, the placement of DRs and OBSs across the network, the tilt of the DR to establish LoS to all or considerably large portions of the network, and the uplink and downlink data rate distribution according to the location of a mobile station and OBS. We believe this is the first work that discusses the use of the orientation of the DR to increase the minimum data rate in the covered area of the OLAN. Our approach provides a mathematical model to estimate the angle of incidence for transmissions in the covered area for a given DR orientation.

3. System configuration and model

The ID-FSOC framework is simple and can be easily modified to suit different environments. We show the key system parameters that affect the performance of the network and that must be considered during its configuration.

3.1. System configuration

Our framework includes the existing last-mile access infrastructure provided by Internet service providers in our design as backhaul Internet access for mobile and stationary stations that communicate in this setting. To simplify our model, but without losing generality, we consider an urban street where DRs and OBS are attached to existing infrastructures such as light posts, traffic posts, signposts, and buildings [31], and an OBS connected to the last-mile access that provides high-speed Internet access for the area covered by the light reflected by these DRs.

An OBS is installed between two identical DRs to provide a downlink response to uplink requests from mobile stations in the coverage area of the DR. Mobile stations in communication with the OBS direct their OTs toward the current DR to establish an uplink, that is, communication from a mobile station to the OBS, and a downlink, that is, communication from the OBS to the mobile station. The ATP mechanism of the mobile stations must be capable of maintaining a LoS to the DR, and is necessary for a continuous exchange of data while they are in motion. The mobile stations are equipped with at least two OTs to enable seamless handovers between DRs; a communicating OT and a handover OT. While the communicating OT is in use, the handover acquires, tracks, and points to the next DR in the path of the moving mobile station. For instance, while the communication link is established on DR-A by the communicating OT, the handover OT locates DR-B for the upcoming handover. Fig. 1 shows an example of the positioning of DR-A and DR-B.

In our model, the OBS is positioned equidistant from two DRs. The OBS has two OTs pointed toward the DRs to which it aims a laser beam as downlink, and it receives a reflected beam as an uplink. Each OT is independent in its operation and dedicated to the DR it faces. The OBS is connected to the last-mile access in the vicinity of the OLAN.

Table 1
Notations used in this paper.

Notation	Description
P_t	Power of the transmitted light
P_0	Power of the transmitted light at a distance
P_r	Power of the reflected light
P	Power of the received light
B	Data rate
d_0	Travel distance
o	Horizontal distance
h	Vertical distance
θ	Angle of incidence
δ	The tilt angle of the DR
δ_H^+	Horizontal tilt of the DR in the clockwise direction
δ_H^-	Horizontal tilt of the DR in the counterclockwise direction
δ_V^+	Vertical tilt of the DR in the clockwise direction
δ_V^-	Vertical tilt of the DR in the counterclockwise direction
δ_{hor}	The horizontal tilt angle of the DR in a dual-plane tilt
δ_{ver}	The vertical tilt angle of the DR in a dual-plane tilt

The mobile stations can easily align their ATP in vehicular networks through the use of a beacon signal [33,34]. This control system then points the transceiver in the direction of the beacon light. In our setup, the beacon signal source is attached to the top center of a DR and transmits a laser beam onto the top of the DR. The mobile station then points the transceiver towards the direction of the beacon signal (that is, the surface of the DR) to transmit and to receive transmissions. Because the DR and OBS are stationary and the corresponding OT of the OBS is pointed to the surface of the DR during installation; hence, no mobility tracking is needed. The wavelength of the proposed beacon signal is 850 nm [33] and is different from the wavelength used for data exchange. Table 1 lists the terms and notations used in this paper.

3.2. System model

Uplink model: This link model is also applicable to the transmitted light from an OBS. By Lambertian law on atmospheric transmission [35], the power of transmitted light P_t at a distance (d) in km (i.e., the distance between transmitter and surface of DR), which we refer to as the incident power P_0 of the light at the DR, can be expressed as

$$P_0 = P_t\, e^{-\gamma d}, \tag{1}$$

where γ is the extinction coefficient that accounts for the deterioration of P_t as a result of the absorption and scattering in the atmosphere. While absorption due to water or water vapor affects

most wavelengths between 1300-1400 nm, the impact of absorption due to atmospheric gases varies for different wavelengths, except for 650 nm, which is immune [36]. Scattering may result from aerosol, smoke, or weather conditions such as fog, snow, and clouds [36,37]. Here, γ, in dB\km, is computed for different atmospheric conditions using Kim's model [38]:

$$\gamma = (\frac{3.91}{v})(\frac{\lambda}{550})^{-q}, \tag{2}$$

where v is the visibility range in km, λ is the wavelength in nm, and q is the size distribution of the scattering particles.

$$q = \begin{cases} 1.6, & \text{high visibility } (v > 50) \text{ km} \\ 1.3, & \text{average visibility } (6 < v \leq 50) \text{ km} \\ 0.16v + 0.34, & \text{hazy visibility } (1 < v \leq 6) \text{ km} \\ v - 0.5, & \text{mist visibility } (0.5 < v \leq 1) \text{ km} \\ 0, & \text{fog visibility } (0.01 < v \leq 0.5) \text{ km} \end{cases} \tag{3}$$

The DR is a Lambertian surface that reflects light with equal power to any angle smaller than 90° from the DR's normal. The power of the reflected light, P_r, is calculated using the Lambert's cosine law on θ, where θ is the angle between the normal of the DR to the point of incidence of the light. The law states that "the intensity varies as the cosine of the incident angle of the light upon the object viewed" [35], and this expression is represented as:

$$P_r = P_0 R \cos\theta, \tag{4}$$

where R is the reflectance of the material used as the DR.

Lambertian law also states that "the power of light is inversely proportional to the square of the distance of the observer to the source" [35]. Hence the power of light received, P, by an observer (mobile station or OBS) at a distance d from the DR can be expressed as:

$$P = \frac{P_r}{d^2\,\pi} \implies P = \frac{P_0\,R\cos\theta}{d^2\,\pi} \tag{5}$$

For the proposed configuration, a mobile station/OBS uses its OTs to transmit a narrow laser beam, with a width of 1 mrad, onto the DR. The beam diameter at the DR makes a surface area S_t on the DR based on the distance between the transmitter and the DR. Likewise, the receiving mobile station/OBS pointing to the DR receives the reflected transmissions from the surface of the DR to where the lens is focused. Here, the size of the area the lens of the receiver focuses S_r is dependent on the aperture area A_r of the photodiode lens and d between the DR and the receiver; that is:

$$S_r = \frac{A_r\,d}{f_r\cos\theta_r}, \tag{6}$$

where f_r is the focal length of the lens and θ_r is the angle between the normal of the DR and the LoS from the center of the lens [13]. The area of the region $d\sigma$ where the S_t and the S_r intersect is critical in establishing the strength of the communication link, or:

$$P = \int_{S_t \cap S_r} \frac{P_0\,R\cos\theta\,A_r}{S_t\,d^2\,\pi} d\sigma \tag{7}$$

Because the intensity of the transmitted beam also depends on the beam diameter, we consider a narrow laser beam for transmissions, such that the resulting S_t from the transmitter is smaller than the S_r in the focus of the receiver (i.e., $S_t << S_r$). The photodiode used by the receiver has $A_r << d$ [13,16,32]. Hence, the power of light received P becomes:

$$P = \frac{P_0\,R\cos\theta\,A_r}{d^2\,\pi} \tag{8}$$

The key factors affecting the OLAN configuration are those associated with the received power, as shown in (8). Both OBS and mobile stations transmit with the same P_t, which can be selected by considering the largest value θ, which is $< 90°$, the farthest d to the DR, and the minimum data rate required in the network. The attenuation loss due to distance for the transmit power P_t is such that $P_t < 0.2$ dB/km for wavelengths between 780 and 1600 nm [39] in high visibility weather. Therefore, the wave propagation loss may be negligible in our system. The factor A_r is fixed for an OT and depends on the OT's manufacturer specifications. The other factors of importance are R, θ, and d. These factors are discussed below.

3.2.1. Reflectance (R) of a DR material

Reflectance or the reflective coefficient of a DR is the ratio of the amplitude of the reflected light from the DR and the amplitude of the incident light. Janecek et al. [17,18] provided a normalized measurement of the reflectance of common materials such as aluminum foil, polytetrafluoroethylene (PTFE) tape, titanium dioxide paint, teflon, lumirror, and tyvek. These materials are suitable for their use as DR in our proposed system. The measured R of materials ranges from 0.78-1.00. The reflectance may sharply decline for some wavelengths, therefore, the material used as DR is selected according to the used wavelength.

3.2.2. The angle of incidence and distance to DR (θ and d)

This angle determines whether there is partial or no reflection of a transmission towards the DR. A transmission with $\theta = 0,\ 30,\ 60$ and 90° achieves 100, 86.7, 50, and 0% reflection of the transmission, respectively. Mobile stations with $\theta \geq 90°$ have no LoS to the DR and receive no reflected light, whereas all other mobile transmissions for which $\theta < 90°$ receive a fraction of P_t. The distance d varies because the mobile station moves. Therefore, θ and d are affected by the location of the DR; mainly by the height difference between the mobile station's OT and the DR (vertical distance h), the lateral distance between the DR and the mobile station's OT (horizontal distance o), and the distance between the DR and the mobile station's OT (travel distance d_0) as if they were in the same plane.

Fig. 2 shows the considered network configurations of an OLAN. In Fig. 2(a), the DR is located in front of a mobile station, so that a moving mobile station travels in a parallel direction to the DR's normal or what we refer to as perpendicular displacement configuration (PDC). In Fig. 2(b), the DR is located at the side of a mobile station, so that the mobile station travels in a perpendicular direction of the DR's normal, or what we refer to lateral displacement configuration (LDC). These figures show the distances d_0, o, and h for PDC and LDC, respectively. We use these two displacement models to estimate the angle of incidence of both an uplink and downlink transmissions across the network.

A negative h (i.e., $-h$) depicts the center of the mobile station's OT is above the DR's center; otherwise, the center of the mobile station's OT is below the DR's center. Likewise, a negative d_0 (i.e., $-d_0$) depicts the center of the mobile station's OT to the left DR's center; otherwise, the center of OT is to the right of the DR's center. Here, θ in Fig. 2, is computed using the cosine rule as:

$$\theta = \arccos(\frac{\overline{OE}^2 + \overline{OC}^2 - \overline{CE}^2}{2\,\overline{OE}\,\overline{OC}}) \tag{9}$$

that is,

$$\theta = \arccos(\frac{d_0^2 + d^2 - i^2}{2d_0 d}), \quad d_0 \neq 0,\ d \neq 0 \tag{10}$$

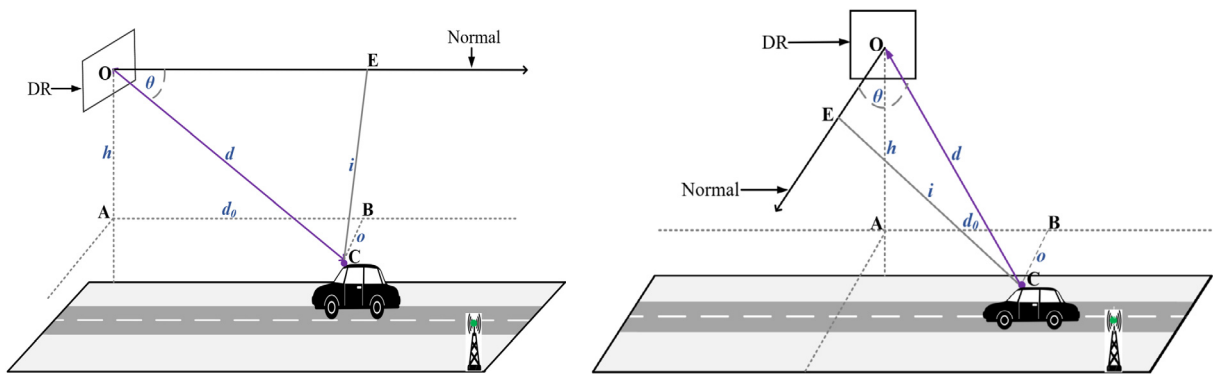

(a) Perpendicular displacement configuration (PDC). (b) Lateral displacement configuration (LDC).

Fig. 2. Basic configuration models of an OLAN.

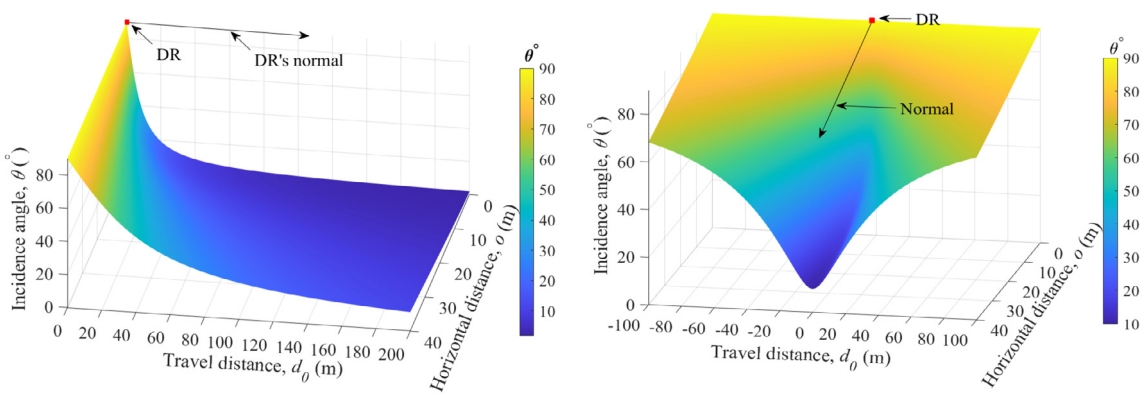

(a) Angle of incidence θ as a function of d_0 and o for PDC. (b) Angle of incidence θ as a function of d_0 and o for LDC.

Fig. 3. Angle of incidence θ as a function of d_0 and o.

for PDC and

$$\theta = \arccos\left(\frac{o^2 + d^2 - i^2}{2od}\right), \quad o \neq 0,\ d \neq 0 \tag{11}$$

for LDC. The angles $\angle EOA = \angle OAB = \angle ABC = 90°$ in both setups. The line segment $\overline{OE} = \overline{AB}$ in PDC, and the segment $\overline{OE} = \overline{BC}$ in LDC.

The expression to compute d is common for PDC and LDC, whereas i is an artifact that is computed using unique expressions for PDC and LDC. The distance d between the center of DR and the center of the OT used in the calculation of the received power can be calculated as:

$$\begin{aligned} &\overline{OC} = (\overline{AB}^2 + \overline{BC}^2 + \overline{AO}^2)^{\frac{1}{2}} \\ &\quad or \\ &d = (d_0^2 + o^2 + h^2)^{\frac{1}{2}} \end{aligned} \tag{12}$$

Here, i is the diagonal of a right angled triangle formed by a vertical line from point E and the intersecting line from point C. The length of i is computed as:

$$\begin{aligned} &\overline{CE} = (\overline{BC}^2 + \overline{AO}^2)^{\frac{1}{2}} \\ &\quad or \\ &i = (o^2 + h^2)^{\frac{1}{2}} \end{aligned} \tag{13}$$

for PDC and

$$\begin{aligned} &\overline{CE} = (\overline{AB}^2 + \overline{AO}^2)^{\frac{1}{2}} \\ &\quad or \\ &i = (d_0^2 + h^2)^{\frac{1}{2}} \end{aligned} \tag{14}$$

for LDC, respectively.

The value of $\theta = 90°$ when the OT of the station is underneath the DR, that is, the case $a - b$ in (15). The value $\theta = 0°$ when the OT is at the center if the DR, that is, the case c in (15), an unlikely scenario for ID-FSOC.

$$\theta = \begin{cases} a)\ 90°, & d_0 = 0 \text{ in PDC} \\ b)\ 90°, & o = 0 \text{ in LDC} \\ c)\ 0°, & d = 0 \text{ in both PDC and LDC} \end{cases} \tag{15}$$

Because the DR location is fixed, we examine the impact of d_0 and o on θ for PDC and LDC uplink transmissions. In both setups, the vertical distance between the DR and the OTs of the mobile stations is 3 m. The DR in both setups provide coverage for a network of area $d_0 \times o = 200 \times 40$ m^2. This area and setup are used in the remaining of the paper unless stated otherwise.

We estimate θ as a function of d, d_0 and o and use i according to (13) and (14) for PDC and LDC, respectively. Fig. 3(a) shows that θ decreases as d_0 increases and it slightly increases as o increases for PDC. The continuous decline in the value of θ as d_0 increases implies a strong P_r.

Conversely, θ increases as d_0 increases while it slightly decreases as o increases in the case of LDC, as shown in Fig. 3(b). The distribution of θ for an increasing d_0 in LDC implies that transmissions from mobile stations that are far from the DR results in a low P_r. As a result, the average P_r in LDC is smaller than that in PDC.

Fig. 3(a) shows at least 80% of covered area in PDC occurs when $\theta \leq 60°$. This result is different from Fig. 3(b) in LDC, which has up to 20% of the covered area with $\theta \leq 60°$. However, both figures show coverage areas with $\theta \cong 90°$ as $d_0 \cong 0$ m for PDC, and $o \cong 0$

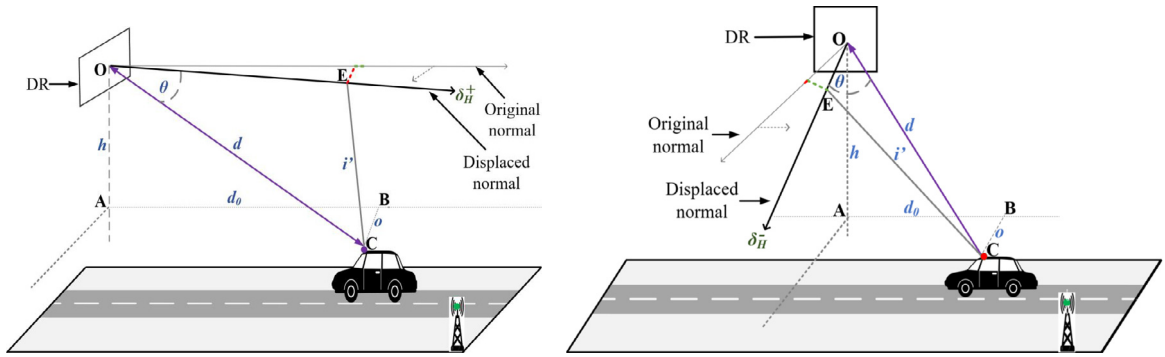

(a) Horizontally tilted DR in PDC setup. (b) Horizontally tilted DR in LDC setup.

Fig. 4. Horizontally tilted DR.

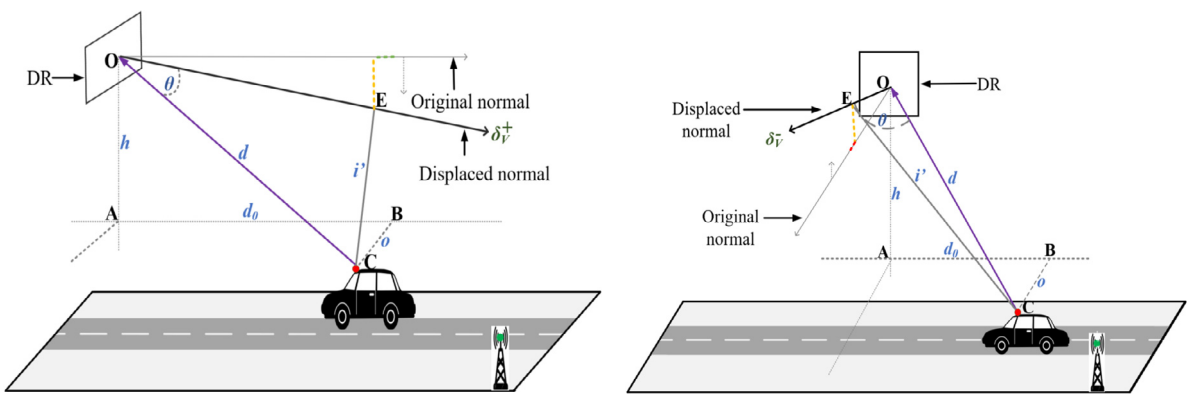

(a) Vertically tilted DR in PDC setup. (b) Vertically tilted DR in LDC setup.

Fig. 5. Vertically tilted DR.

m for LDC. Mobile stations in regions with $\theta \cong 90°$ may not be able to communicate because they lack LoS to the DR, that is, $P_r \cong 0$ and $P \cong 0$.

In general, as θ increases, P_r decreases, and as θ decreases, P_r increases. A tilt of the DR toward a region in the covered area displaces the DR's normal in the direction of the tilt, which results in an increase of P_r for the mobile stations in that region. The increase of P_r by a tilt decreases P_r in other regions of the covered area as the DR's normal moves away. The tilt angle of a DR (δ) is the angle between the original position of the normal and the current position of the normal (referred to as the displaced normal) after a tilt of the DR.

4. Increasing the LoS in the covered area

Here, we propose a mathematical model to estimate θ when the DR is tilted. Using this model, we use the RISE algorithm to compute the near optimal tilt angle of the DR. We also examine the increase in LoS and the minimum P_r from tilting the DR towards the covered area.

4.1. Estimation of θ after a tilt of the DR

The DR can be tilted vertically, with reference to h, or horizontally, with reference to d_0. A vertical tilt of the DR produces a displaced normal above or below the original normal. We refer to a vertical tilt with the displaced normal above the original normal as a vertical counterclockwise tilt. Likewise, we refer to a vertical tilt with the displaced normal below the original normal as vertical clockwise tilt. A horizontal tilt of the DR produces a displaced normal to the left or right of the original position of the normal. In a horizontal counterclockwise tilt, the displaced normal is at the right of the original normal, whereas, in a horizontal clockwise tilt, the displaced normal is as the left of the original normal.

The tilt in either the horizontal and vertical axis is in the range 0-90°. The tilt of the DR in a horizontal clockwise, horizontal counterclockwise, vertical clockwise, and vertical counterclockwise direction are denoted as δ_H^+, δ_H^-, δ_V^+, and δ_V^-, respectively.

Fig. 4 shows a δ_H^+ for PDC and δ_H^- for LDC. Here, the length of the segments $\overline{OE}$ and $\overline{OC}$ remain the same after the tilt and the changes in o, d_0, and h are indicated with dashed red, green, and orange lines, respectively. As shown in the figure, d_0 and o change after the tilt, which in turn changes i (i.e., segment $\overline{CE}$ or i') in both setups. In a horizontal tilt of the DR, i' is calculated as:

$$i' = [(d_0 - d_0 \cos\delta)^2 + (o - \psi_H d_0 \sin\delta)^2 + h^2]^{\frac{1}{2}} \quad \text{for PDC} \tag{16}$$

and

$$i' = [(d_0 + \psi_H o \sin\delta)^2 + (o - o\cos\delta)^2 + h^2]^{\frac{1}{2}} \quad \text{for LDC} \tag{17}$$

where $\psi_H = \{1, -1\}$ for δ_H^+ and δ_H^-, respectively.

Fig. 5 shows that δ_V^+ in PDC produces a change in both h and d_0, which in turn changes i. On the other hand, δ_V^- in LDC produces a change in h and o, which in turn changes i. The calculation of i' in a vertical tilt of the DR follows:

$$i' = [(d_0 - d_0 \cos\delta)^2 + o^2 + (h - \psi_V d_0 \sin\delta)^2]^{\frac{1}{2}} \quad \text{for PDC} \tag{18}$$

and

$$i' = [d_0^2 + (o - o\cos\delta)^2 + (h - \psi_V o \sin\delta)^2]^{\frac{1}{2}} \quad \text{for LDC} \tag{19}$$

where $\psi_V = \{1, -1\}$ for δ_V^+ and δ_V^-, respectively.

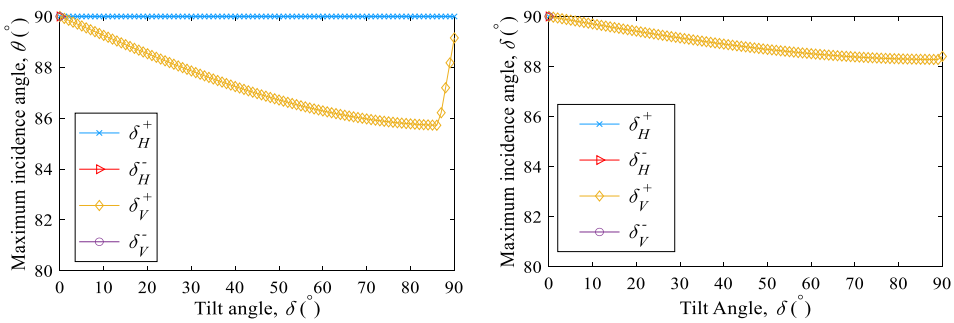

(a) Largest θ for different tilts of the DR for PDC. (b) Largest θ for different tilts of the DR for LDC.

Fig. 6. Graph showing the largest θ for different tilts of the DR.

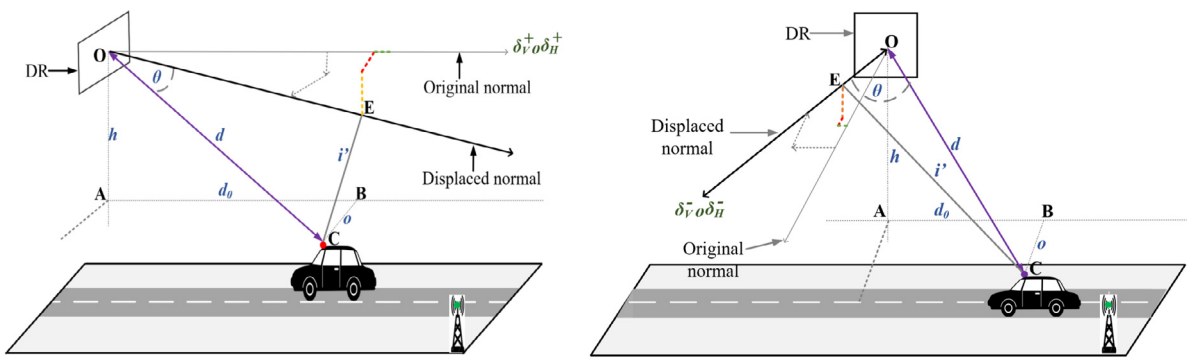

(a) $\delta_H^+ \circ \delta_V^+$ PDC setup. (b) $\delta_H^- \circ \delta_V^-$ LDC setup.

Fig. 7. Horizontal and vertical tilting of the DR.

We estimate the largest θ after a tilt of the DR for both setups. Here, a decrease in the largest θ implies that the tilt of the DR increases P_r in regions where P_r was previously weak. Conversely, an increase in the largest value of θ implies the tilt of the DR exacerbates an already small P_r. Figs. 6(a) and 6(b) show the largest value of θ after the tilt of the DR in PDC and LDC, respectively.

Here, δ_H^- and δ_V^- in PDC should be avoided because the largest $\theta > 90°$, as shown in Fig. 6(a). These tilts reduce the size of the covered area. δ_H^+ produces no changes in the largest θ, whereas δ_V^+ achieves the desired result, that is, $\theta = 85.7°$ at $\delta = 86°$. Fig. 6(b) shows that δ_H^+, δ_H^- and δ_V^- must be avoided in LDC. On the other hand, δ_V^+ of the DR is a tilt in the right direction because it produces a large $\theta < 90°$, that is, $\theta = 88.3°$ for a $\delta = 89°$.

The orientation of a DR might be a combination of vertical and horizontal tilts. We refer to such a tilt as a dual-plane tilt. Here, we consider a vertical tilt followed by a horizontal tilt. The tilt of the DR is either δ_V^+ or δ_V^-, and δ_H^+ or δ_H^- in both setups. Figs. 7(a) and 7(b) show a $\delta_H^+ \circ \delta_V^+$ and $\delta_H^- \circ \delta_V^-$ dual-plane tilt for PDC and LDC, respectively. As shown by the dashed lines, the dual-plane tilt of the DR affects only the computation of i in both setups when the lengths of the segments $\overline{OE}$ and $\overline{OC}$ remain the same after the tilt. Let us denote the horizontal and vertical tilt angles of the DR in a dual-plane tilt as δ_{hor} and δ_{ver}, respectively, then in a dual-plane tilt of the DR, i' is computed as follows:

$$i' = [(d_0 - d_0 \cos\delta_{ver} \cos\delta_{hor})^2 + (o - \Psi_H d_0 \cos\delta_{ver} \sin\delta_{hor})^2 + (h - \Psi_V d_0 \sin\delta_{ver})^2]^{\frac{1}{2}} \tag{20}$$

for PDC and

$$i' = [(d_0 + \Psi_H o \cos\delta_{ver} \sin\delta_{hor})^2 + (o - o \cos\delta_{ver} \cos\delta_{hor})^2 + (h - \Psi_V o \sin\delta_{ver})^2]^{\frac{1}{2}} \tag{21}$$

for LDC.

4.2. Near optimal tilt angles of the DR

Let us denote X as the set of OTs of the mobile stations and the OBSs that communicate through a DR denoted as y, where $x \in X$ is an OT that communicates through y. If H is the set of vertical distances of the OTs, $h \in H$ is the index of the vertical distance of OT x (i.e., h_x). Let us denote L as the region $\{d_0 \times o\}$ covered by DR y, where $l \in L$ is the index of an OT in L (i.e., l_x). OT x with LoS to DR y has $\theta_{xy} < 90°$. Conversely, OT x without LoS to DR y has $\theta_{xy} \geq 90°$. Let us denote $\Omega_{xy} = 1$ as OT x with LoS to DR y, and $\Omega_{xy} = 0$ otherwise. The optimization expression of the maximum number of OTs that communicate through a tilted DR is given as:

$$\begin{aligned} &\arg\max_{l_x, h_x} \sum_{x \in X} \Omega_{xy} \\ &\quad \textit{subject to} \\ &C1: \ \theta_{xy} < 90°, \forall x \in X \\ &C2: \ 0 \leq \delta_{ver} \leq 90° \\ &C3: \ 0 \leq \delta_{hor} \leq 90° \end{aligned} \tag{22}$$

Constraint C1 ensures LoS between the communicating OTs and the DR. Constraints C2 and C3 define the vertical and horizontal tilts of the DR that maximize the LoS across the network.

Here, the optimal tilt of the DR enables the largest number of communicating OTs in the covered area. The placement of the DR and the associated dual-plane tilt are similar to the three-dimension cell deployment of a drone base station, known to be NP-hard [40–42]. Therefore, we propose the RISE algorithm to maximize the number of OTs that communicate through the DR. Algorithm 1 describes RISE as a pseudocode. The location of the DR is assumed to be known before the DR is tilted. In RISE, the covered area is divided into cells, and θ is computed over each cell

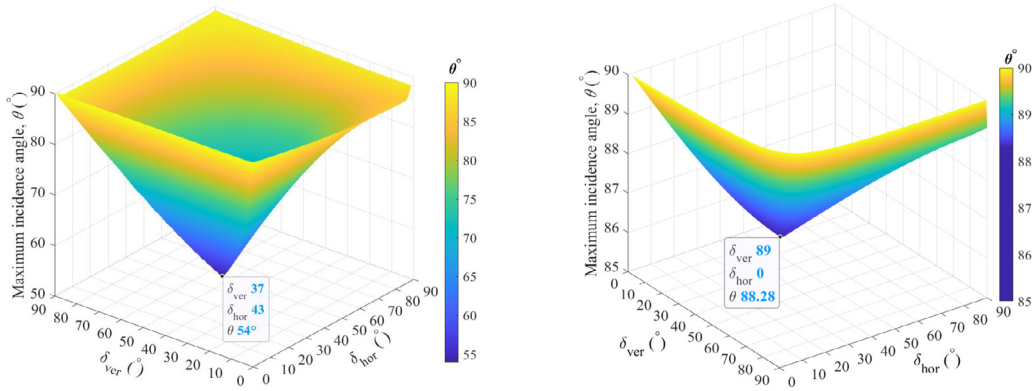

(a) Largest θ as a function of δ_hor and δ_ver for PDC.

(b) Largest θ as a function of δ_hor and δ_ver for LDC.

Fig. 8. Largest θ as a function of δ_hor and δ_ver.

after every dual-plane tilt of the DR. The value of θ is computed on the minimum and maximum h_x in each cell to account for the different vertical distances of OTs that may pass through those cells as the mobile stations move. Records of the largest θ and the associated δ_{ver} and δ_{hor} are stored for each dual-plane tilt; and the near optimal dual-plane tilt angles of the DR are the values of δ_{ver} and δ_{hor} associated to the smallest of the largest θ obtained from the stored records after θ is computed for all possible dual-plane tilts of the DR. The computation of the largest θ for a dual-plane tilt terminates when the largest θ computed is $\geq 90°$ in any of the cells.

Algorithm 1 RISE algorithm.

1: $h_{min} \leftarrow$ *Gets the minimum vertical distance*;
2: $h_{max} \leftarrow$ *Gets the maximum vertical distance*;
3: $d_{0max} \leftarrow$ *Get the travel distance of the covered area*;
4: $o_{max} \leftarrow$ *Get the horizontal distance of the covered area*;
5: $opt_{hor} = -1,\ opt_{ver} = -1,\ min_{ang} = 90$;
6: **while** $\delta_{ver} \leq 90$ **do**
7: **while** $\delta_{hor} \leq 90$ **do**
8: $net_{max} = 0$;
9: **while** $o \leq o_{max}$ **do**
10: **while** $d_0 \leq d_{0max}$ **do**
11: *var1 = compute* θ *for* h_{min};
12: *var2 = compute* θ *for* h_{max};
13: $\theta = max(var1, var2)$;
14: **if** $\theta \geq 90°$ **then**
15: $min_{ang} = 90°$;
16: *go to 7*;
17: **else if** $\theta > net_{max}$ **then**
18: $net_{max} = \theta$;
19: **if** $net_{max} < min_{ang}$ **then**
20: $min_{ang} = net_{max}$;
21: $opt_{hor} = \delta_{hor}$;
22: $opt_{ver} = \delta_{ver}$;
23: **if** $min_{ang} < 90$ **then**
24: *Near optimal* $\{\delta_{hor}, \delta_{ver}\} = \{opt_{hor}, opt_{ver}\}$;
25: **else**
26: *No near optimal tilt angles found*;

Figs. 8(a) and 8(b) show the largest θ for $\delta_H^+ \circ \delta_V^+$ using the RISE algorithm for PDC and LDC, respectively. As shown in the figures, the smallest of the maximum θ are 54° and 88.3° for PDC and LDC, respectively. The $\{\delta\_hor, \delta\_ver\}$ that correspond to the smallest θ, that is, the near optimal dual-plane tilt angles, are {43°, 37°} for PDC and {0°, 89°} for LDC. A comparison between Figs. 8 and 3 shows that the largest value of θ for both setups can be decreased from 90° to 54° and 88.3° for PDC and LDC, respectively, by tilting the DR. This tilt also guarantees reflections for all the transmissions towards the DR. The algorithm computes δ_H^+ and δ_V^+ because $\theta \leq 90°$ for those tilts in PDC, as shown in Fig. 6. If no optimal tilt angles are found, the location of the DR may be changed and the optimal tilt angles are recomputed using the algorithm.

4.3. Increase in LoS and the minimum P_r after a DR tilt

Figs. 9(a) and 9(b) show the incidence angle for transmissions in the covered area for both setups, after a near optimal tilt of the DR. The near optimal tilt of the DR increases the LoS to 100% in 9(a) and 9(b) as compared to that in Figs. 3(a) and 3(b), where some regions have no LoS, or $\theta \cong 90°$.

We computed the uplink P_r in high visibility weather using (4) on the estimated values of θ in Figs. 9(a) and 9(b). R and P_t used in the computation of P_r are 1 and 100 mW, respectively. Figs. 10(a) and 10(b) show P_r of the transmissions across the covered area for PDC and LDC, respectively. From the graphs, P_r increases as θ decreases, and vice versa. The minimum, average, and maximum P_r obtained are {60.2, 73.6, 100} mW and {7, 17.2, 100} mW, respectively. PDC shows that 100% of the transmissions in the covered area have $\theta \leq 60°$; or an increase of about 12%. On the other hand, LDC shows a 15% decrease in the covered area where $\theta \leq 60°$. Despite the decrease in the covered area, where $\theta \leq 60°$, both setups achieve $P_r > 0$ mW as a result of the tilt.

5. Data rate and noise reduction

DR positioning in both setups affects the size and location of the covered area that experience a given data rate. We performed numerical evaluations on the received power and data rate for the proposed optical network using the smallest P_r obtained using the near optimal tilt algorithm. The targeted minimum bit error rate (BER) for our simulation is 10^{-9} for a link 15.56 dB signal-to-noise ratio (SNR). We consider parameters similar to those in [16], where the OT receiver is a Mercury Cadmium Telluride (HgCdTe) avalanche photodiode (APD) with high sensitivity to wavelengths at 1550 nm. The receiver responsivity (ρ) is 0.8 A/W and the aperture of the receiving lens is 9.5×10^{-3} m^2. The required number of photons to achieve a BER of 10^{-9} for SNR=15.56 dB is at least 57. The modulation scheme considered is on-off-keying non return-to-zero (OOK-NRZ).

We analyze the received power at different points in the covered area and then translate the received power into the corresponding data rates. The smallest P_r in Figs. 10(a) and 10(b) are used to evaluate P for PDC and LDC and the corresponding data rates. The received power is shown in Figs. 11(a) and 11(b) for PDC and LDC, respectively. The graphs show that P is the largest at the DR located at $\{d_0, o\} = \{0, 0\}$ m and it decreases as the distance from the DR increases. As expected, the inverse relationship between d and P results in the decline of P as d increases.

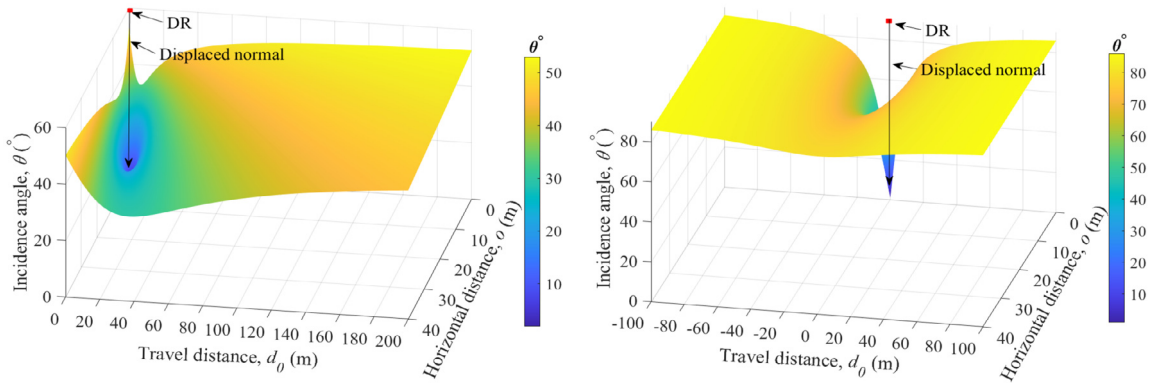

(a) Angle of incidence θ after a near optimal tilt of the DR for PDC. (b) Angle of incidence θ after a near optimal tilt of the DR for LDC.

Fig. 9. Angle of incidence θ after a near optimal tilt of the DR.

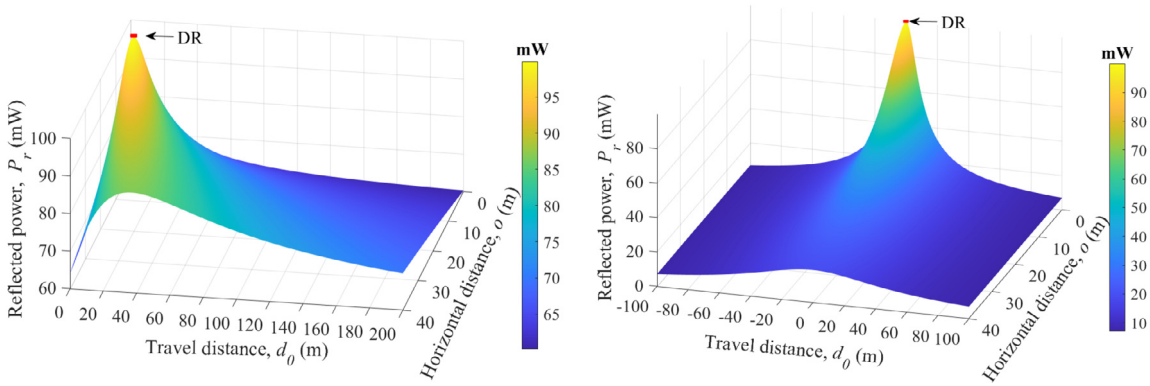

(a) Reflected power P_r in mW as a function of d_0 and o in PDC. (b) Reflected power P_r in mW as a function of d_0 and o in LDC.

Fig. 10. Reflected power P_r as a function of d_0 and o.

5.1. Data rates in the covered area

The data rate (B) is defined in terms of P as

$$P = \frac{N_p \hbar c B}{\lambda}, \tag{23}$$

in the considered setups where N_p is the average number of photons for a single information bit, $\hbar$ is Planck's constant, and c is the speed of light.

Figs. 11(c) and 11(d) show the received power as the achievable data rates of {1, 10, 20, 50, 100} Gbps for PDC and LDC, respectively. As shown in the two figures for the considered setups, the decrease in data rates is caused by the decrease in the value of P to the DR. The smallest data rate determines the maximum value of d_0 and o in the covered area. For a minimum data rate of 1 Gbps in the covered area, the largest distance away from the DR for $\{d_0, o\} = \{154, 40\}$ m for PDC setup and $\{d_0, o\} = \{38, 40\}$ m for LDC setup. LDC produces a smaller covered area with $B \geq 1$ Gbps as compared to PDC because of its minimum P_r, which is about 12% of the minimum P_r in PDC.

5.2. Outage probability and bit error rate (BER)

The outage region refers to parts of the covered area where the minimum data rate cannot be achieved. The minimum power P_{min} required at the receiver to correctly decode a 1 Gbps transmission is -51.4 dBm. This implies, $P < P_{min}$ in the outage region. The outage probability P_{out} can be written as:

$$P_{out} = P < P_{min} \tag{24}$$

The bit error rate (BER) in ID-FSOC is given as [43]:

$$BER = \text{erfc}(N_p \hbar c \rho / 2q)^{\frac{1}{2}} \tag{25}$$

where erfc is the complementary error function and q is the charge of an electron. Figs. 12(a) and 12(b) show the outage probability and the BER as a function of d_0 for PDC and LDC, respectively. As shown in the graphs, the outage probability increases as P continue to decrease below P_{min} due to increasing d_0 in both setups. Likewise, the BER in both setups increases as P decreases with an increase in d_0. The decrease in P implies a decrease in the number of photons reaching the receiver. These results show that the BER is remarkably low so that large data rates are achievable at moderate travel distances. PDC provides higher minimum P_r than LDC and that implies that mobile stations can transmit at higher data rates in PDC. Also, the covered area in PDC is wider than that in LDC, and that reduces the required number of DRs and OBSs in PDC to set a large OLAN.

5.3. Sunlight noise in outdoor environments

ID-FSOC faces many challenges to make it feasible for deployment. Some of those are using receivers sensitive enough and noise. In outdoor scenarios, sun radiation is a major source of noise. Luckily, there are different well-known techniques to diminish such noise: filters [44], casing, and shading (awning). Being the last the simplest technique, we experimentally look into the spectrum observed in the reflected light on paper, used as a diffuse reflector, with simultaneously projected laser light at 532, 655, and 852 nm.

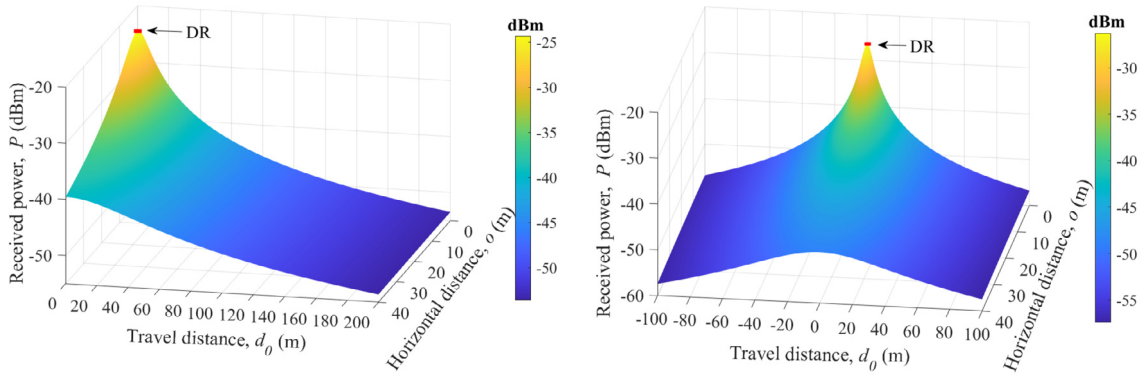

(a) Received power P in dBm using smallest $P_r = 60.2$ mW for PDC.

(b) Received power P in dBm using smallest $P_r = 7$ mW for LDC.

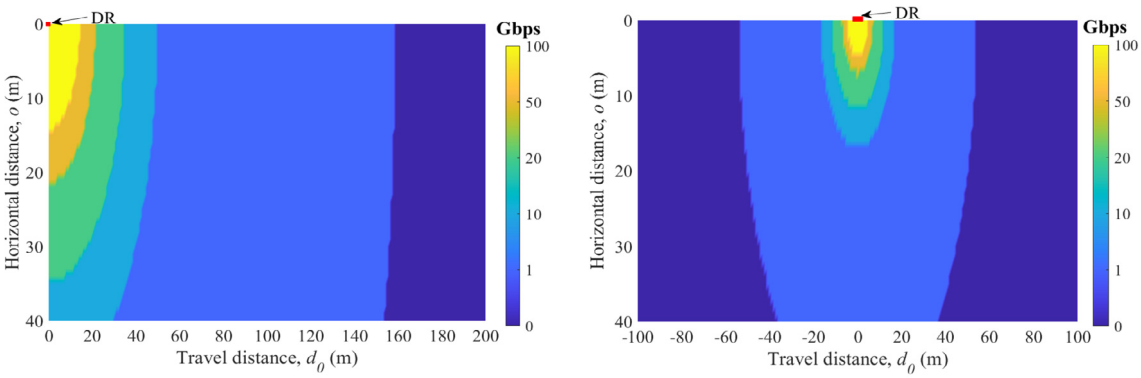

(c) Data rate in Gbps corresponding to P for PDC.

(d) Data rate in Gbps corresponding to P for LDC.

Fig. 11. P and B for PDC and LDC setup.

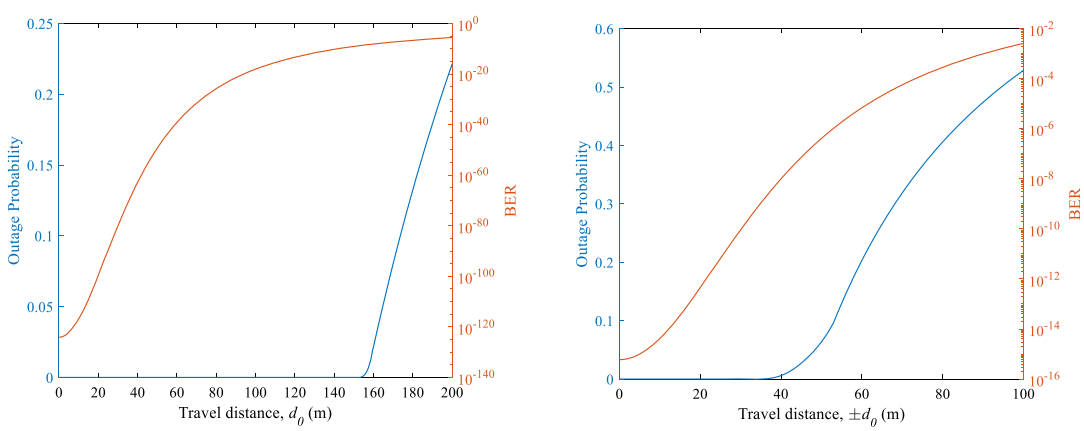

(a) Outage probability and BER for PDC.

(b) Outage probability and BER for LDC.

Fig. 12. Outage probability and BER for PDC and LDC setup.

We recorded the spectrum of the reflected light with direct sun illumination and another with shaded DR (i.e., without direct sunlight) to show the effectiveness of shading. Fig. 13(a) shows the spectrum detected on the exposed DR, i.e., without a shade. The spectrum shows the presence of the laser light with significant intensity and also significant amount of noise around the reflected light. In contrast, a shade can significantly reduce the noise around signal of interest, as Fig. 13(b) shows. In addition and overall, these figures also show that the selection of a wavelength in a less noisy region of the spectrum may simplify the noise filtering process.

For demonstration of diffuse reflection concept, we performed an experiment to measure P from a DR made of Teflon with $R = 0.8$. We transmitted an 852-nm laser beam with $P_t = 1$ W and $\theta = 52°$. Using a S120VC photodiode power sensor connected to a PM400 power and energy meter console, we measured the received power from the DR (i.e., DR_A). Attached to the power sensor is an LC1715-A-ML plano-convex lens that focuses the power sensor to the reflected beam on the DR to the active area of the power sensor. The diameter of the active area of the power sensor is 9.7 mm and $\rho = 38$ mA/W at 852 nm. The measured P in Fig. 14(a) shows a small difference between the estimated P and that of DR_A. We further investigated the effects of other forms of noise, that is, water on DR (DR_B) by spraying water onto the DR's surface, and dirt (DR_C). As shown in Fig. 14(a), P decreases for

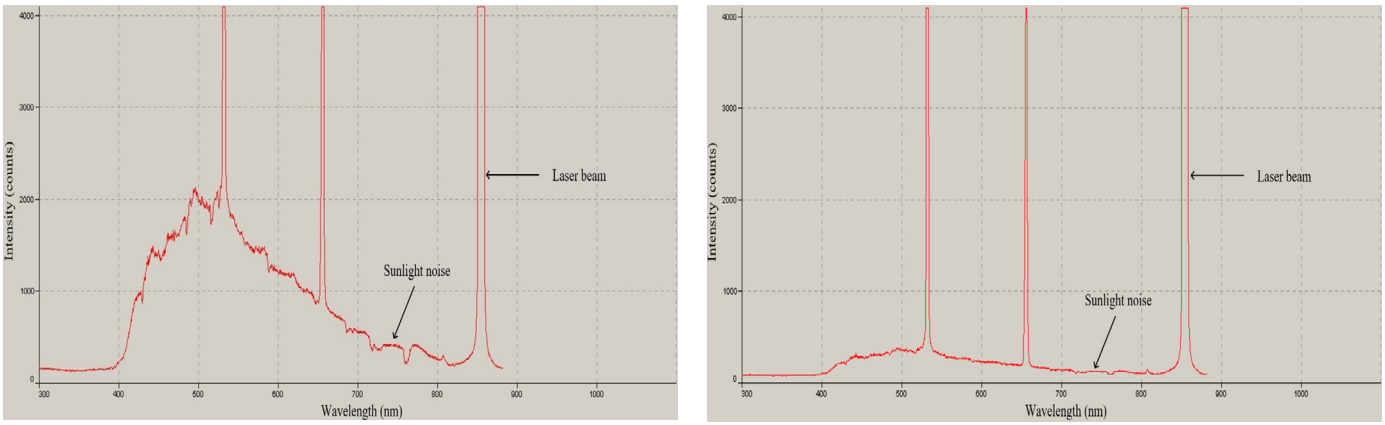

(a) Spectrum of direct and indirect light on an exposed DR. (b) Spectrum of direct and indirect light on a shaded DR.

Fig. 13. Difference in noise between a shaded and exposed DR under sunlight.

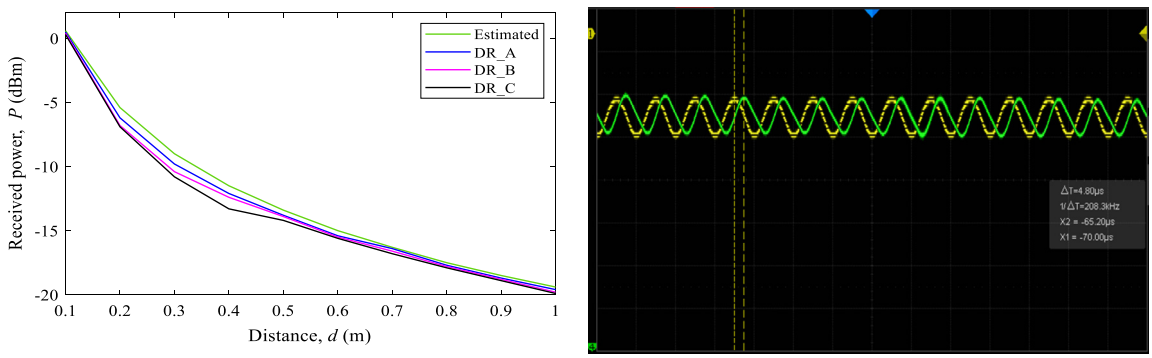

(a) Received power P from a DR under varied conditions. (b) Received signal from a DR.

Fig. 14. Received power and signal from a DR.

both scenarios, with DR_C showing the largest loss. Yet, the difference among these three surfaces is not significant. As for bubbles that may form on the surface for the presence of water, we theorize that the response may be very similar to that of a wet surface. However, confirmation remains for future research.

Strong vibrations experienced by an OT in a moving vehicle might result in a significant shift in the area of focus on the DR, and in turn, it might affect the strength of the received signal as part or all of the reflected beam falls out of the lens' focused view of the receiver. Fortunately, the shift in the focus of the receiver is very small for moving vehicles on tarred roads [45,46]. One possibility to reduce the effect of vibration on the generated pointing error is to increase the diameter of the reflected beam so as to permit vibrations of a given amplitude and continue to hold the established link [47,48]. However, the increase of the beam diameter may come at the cost of a reduced P at the receiver and thus of a reduction of the largest distance between the DR and a receiver.

We also measured the phase shift between a 50 KHz transmitted signal and the received signal. Fig. 14(b) shows the phase difference between the output of the photodetector or the recovered signal (green wave) and the transmitted signal (yellow wave). The measured phase difference between the signals is 4.8 µs. The computed phase shift between the transmitted and received signal is about 86.4°. Fig. 15 shows the setup used in this experiment.

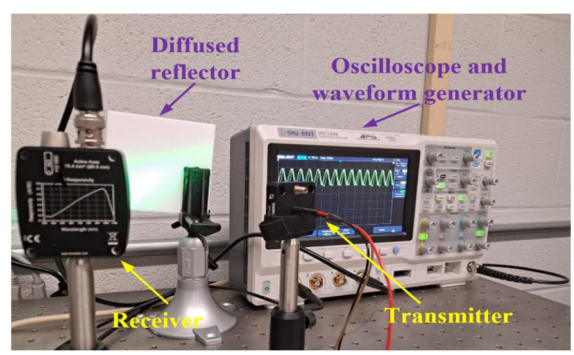

Fig. 15. An optical transmitter and receiver.

6. Conclusions

In this paper, we proposed a model of the tilt of a diffuse reflector and its effects on network access properties in the indirect LoS diffuse light FSOC or ID-FSOC framework of an optical local area network for a vehicular network leverages communications between ground-to-vehicle and vehicle-to-ground. A main difference from conventional free-space optical communications, ID-FSOC enables a broadcast channel and such channel permits not only multiple access but also station mobility.

We modeled and analyzed the effect of a tilt of the DR on the incidence angle, and the effect of the angle of incidence of the incoming light beam in ID-FSOC has on the covered area. In this network, the use of diffuse reflectors eliminates the requirement of having a direct LoS between receivers and transmitters, and that provides several advantages: It a) reduces the complexity of transceiver tracking required to maintain a communication link in FSOC networks; b) increases the beam size in some scenarios and minimizes the complexities involved with the used ATP; c) converts point-to-point optical links into a broadcast channel so

one ground station can communicate with multiple stations; and d) enables network access by mobile stations, such as cars, and the transmission of large data rates. We showed that the proposed network can support data rates of 1 Gbps or greater and the required infrastructure is easy to deploy.

Our heuristic algorithm, RISE, computes the near optimal tilt angles of the DR that extends LoS to regions in the network. This expansion of the covered area minimizes the number of DRs and OBSs required in a large area. We believe this is the first technique to improve the minimum reflected power of an ID-FSOC system using the orientation of the DR. We compared the impact of the DR tilt between the perpendicular and lateral displacement configurations. Our analysis showed that the reflected power, received power, and data rate are higher in a perpendicular displacement configuration than in a lateral displacement configuration, making this configuration of the DR the most suitable for an urban scenario.

We also showed a snapshot of the spectrum around the wavelength that ID-FSOC may use in an actual implementation. Such results show the significant reduction of the noise induced by sun radiation achieved by a shade on a DR in an outdoor scenario. We also showed experimental received power measurements in a controlled laboratory environment.

Declaration of competing interest

The authors declare that they have no known competing financial interests or personal relationships that could have appeared to influence the work reported in this paper.

References

[1] K. Wang, A. Nirmalathas, C. Lim, E. Skafidas, K. Alameh, Free-space optics for high-speed reconfigurable card-to-card optical interconnects, in: Nonimaging Optics: Efficient Design for Illumination and Solar Concentration X, vol. 8834, International Society for Optics and Photonics, 2013, 88340I.

[2] R. Slomski, E. Skedek, Optical communication as a perspective method of exchanging data in dedicated systems, in: Photonics Applications in Astronomy, Communications, Industry, and High-Energy Physics Experiments 2014, vol. 9290, International Society for Optics and Photonics, 2014, 92900C.

[3] J.C. Juarez, K.T. Souza, N.G. Bos, A.M. Brown, B.M. Cannon, K.G. Petrillo, J.L. Riggins II, J.E. Sluz, H.J. Tomey, R.A. Venkat, Lasercomm system development for high-bandwidth terrestrial communications, in: Atmospheric Propagation XIII, vol. 9833, International Society for Optics and Photonics, 2016, 98330A.

[4] S. Chaudhary, A. Amphawan, The role and challenges of free-space optical systems, J. Opt. Commun. 35 (4) (2014) 327–334.

[5] M. Toyoshima, Y. Munemasa, H. Takenaka, Y. Takayama, Y. Koyama, H. Kunimori, T. Kubooka, K. Suzuki, S. Yamamoto, S. Taira, et al., Introduction of a terrestrial free-space optical communications network facility: IN-orbit and Networked Optical ground stations experimental Verification Advanced testbed (INNOVA), in: Free-Space Laser Communication and Atmospheric Propagation XXVI, vol. 8971, International Society for Optics and Photonics, 2014, 89710R.

[6] J. Muth, Free-space optical communications: building a 'deeper' understanding of underwater optical communications, Laser Focus World, May 10, 2017. Online: https://www.laserfocusworld.com/optics/article/16548276/freespace-optical-communications-building-a-deeper-understanding-of-underwater-optical-communications.

[7] C. Casey, Free space optical communication in the military environment, Tech. Rep., Naval Postgraduate School, Monterey, CA, 2014.

[8] J.W. Lai, Free space optical communication for tactical operations, Tech. Rep., Naval Postgraduate School, Monterey, United States, 2016.

[9] H.H. Refai, J.J. Sluss Jr., H.H. Refai, M. Atiquzzaman, Transporting RF signals over free-space optical links, in: Free-Space Laser Communication Technologies XVII, vol. 5712, International Society for Optics and Photonics, 2005, pp. 46–54.

[10] A. Malik, P. Singh, Free space optics: current applications and future challenges, Int. J. Opt. 2015 (2015).

[11] H. Zhang, H. Li, X. Dongya, C. Chao, Performance analysis of different modulation techniques for free-space optical communication system, TELKOMNIKA 13 (2015) 880.

[12] Y. Kaymak, R. Rojas-Cessa, J. Feng, N. Ansari, M. Zhou, T. Zhang, A survey on acquisition, tracking, and pointing mechanisms for mobile free-space optical communications, IEEE Commun. Surv. Tutor. 20 (2) (2018) 1104–1123.

[13] G. Yun, M. Kavehrad, Indoor infrared wireless communications using spot diffusing and fly-eye receivers, Can. J. Electr. Comput. Eng. 18 (4) (1993) 151–157.

[14] D. Wu, Z. Ghassemlooy, S. Rajbhandari, H. Le Minh, A.C. Boucouvalas, Improvement of transmission bandwidth for indoor optical wireless communication systems using an elliptical Lambertian beam, IEEE Photonics Technol. Lett. 25 (2) (2012) 107–110.

[15] W.-C. Wang, C.-W. Chow, L.-Y. Wei, Y. Liu, C.-H. Yeh, Long distance non-line-of-sight (NLOS) visible light signal detection based on rolling-shutter-patterning of mobile-phone camera, Opt. Express 25 (9) (2017) 10 103–10 108.

[16] Y. Kaymak, S. Fathi-Kazerooni, R. Rojas-Cessa, Indirect diffused light free-space optical communications for vehicular networks, IEEE Commun. Lett. 23 (5) (2019) 814–817.

[17] M. Janecek, W.W. Moses, Optical reflectance measurements for commonly used reflectors, IEEE Trans. Nucl. Sci. 55 (4) (2008) 2432–2437.

[18] M. Janecek, Reflectivity spectra for commonly used reflectors, IEEE Trans. Nucl. Sci. 59 (3) (2012) 490–497.

[19] C. Masterson, Massive MIMO and beamforming: the signal processing behind the 5G buzzwords, in: 10 Massive MIMO and Beamforming: The Signal Processing Behind the 5G Buzzwords, 2017, p. 10.

[20] V. Arun, H. Balakrishnan, RFocus: beamforming using thousands of passive antennas, in: 17th {USENIX} Symposium on Networked Systems Design and Implementation ({NSDI} 20), 2020, pp. 1047–1061.

[21] R.C. Short, M.A. Cosgrove, D.L. Clark, P.J. Oleski, Performance of a demonstration system for simultaneous laser beacon tracking and low-data-rate optical communications with multiple platforms, in: Free-Space Laser Communication Technologies III, vol. 1417, International Society for Optics and Photonics, 1991, pp. 464–475.

[22] M. Toyoshima, N. Miyashita, Y. Takayama, H. Kunimori, S. Kimura, System analysis of non-mechanical compact optical transceiver for wireless communications with a VCSEL array, in: 2008 6th International Symposium on Communication Systems, Networks and Digital Signal Processing, IEEE, 2008, pp. 187–190.

[23] N. Hayasaka, T. Ito, Channel modeling of nondirected wireless infrared indoor diffuse link, Electron. Commun. Jpn., Part 1, Commun. 90 (6) (2007) 9–19.

[24] C.B. Liu, B. Sadeghi, E.W. Knightly, Enabling vehicular visible light communication (V2LC) networks, in: Proceedings of the Eighth ACM International Workshop on Vehicular Inter-networking, 2011, pp. 41–50.

[25] D.-R. Kim, S.-H. Yang, H.-S. Kim, Y.-H. Son, S.-K. Han, Outdoor visible light communication for inter-vehicle communication using controller area network, in: 2012 Fourth International Conference on Communications and Electronics (ICCE), IEEE, 2012, pp. 31–34.

[26] I. Takai, T. Harada, M. Andoh, K. Yasutomi, K. Kagawa, S. Kawahito, Optical vehicle-to-vehicle communication system using LED transmitter and camera receiver, IEEE Photonics J. 6 (5) (2014) 1–14.

[27] B. Turan, S. Ucar, Vehicular visible light communications, in: Visible Light Communications, 2017, p. 133.

[28] M. Elamassie, M. Karbalayghareh, F. Miramirkhani, R.C. Kizilirmak, M. Uysal, Effect of fog and rain on the performance of vehicular visible light communications, in: 2018 IEEE 87th Vehicular Technology Conference (VTC Spring), IEEE, 2018, pp. 1–6.

[29] M. Vieira, M. Vieira, P. Louro, P. Vieira, Vehicular visible light communication: a road-to-vehicle proof of concept, in: Optical Sensing and Detection V, vol. 10680, International Society for Optics and Photonics, 2018, 106800J.

[30] J. Zhang, O. Alharbi, T.J. Kane, Simulations of vehicular optical wireless communication systems and comparisons with DSRC systems, Appl. Opt. 60 (20) (2021) E17–E33.

[31] D.F. Wilkins, Optical communications and obstacle sensing for autonomous vehicles, Mar. 26, 2015, US Patent App. 14/034,130.

[32] N. Macaluso, R. Rojas-Cessa, M. Meo, Media access schemes for indirect diffused free-space optical networks, in: 2019 IEEE 40th Sarnoff Symposium, IEEE, 2019, pp. 1–6.

[33] K. Mori, M. Terada, K. Nakamura, R. Murakami, K. Kaneko, F. Teraoka, D. Yamaguchi, S. Haruyama, Fast handover mechanism for high data rate ground-to-train free-space optical communication system, in: 2014 IEEE Globecom Workshops (GC Wkshps), IEEE, 2014, pp. 499–504.

[34] K. Mori, M. Terada, D. Yamaguchi, K. Nakamura, K. Kaneko, F. Teraoka, S. Haruyama, Fast handover mechanism for high data rate ground-to-train free-space optical communication transceiver for internet streaming applications, IEICE Trans. Commun. 99 (5) (2016) 1206–1215.

[35] J.J. Gray, Johann Heinrich Lambert, mathematician and scientist, 1728–1777, Hist. Math. 5 (1) (1978) 13–41.

[36] A.K. Majumdar, J.C. Ricklin, Effects of the atmospheric channel on free-space laser communications, in: Free-Space Laser Communications V, vol. 5892, International Society for Optics and Photonics, 2005, 58920K.

[37] G.-y. Hu, C.-y. Chen, Z.-q. Chen, Free-space optical communication using visible light, J. Zhejiang Univ. Sci. A 8 (2) (2007) 186–191.

[38] I.I. Kim, B. McArthur, E.J. Korevaar, Comparison of laser beam propagation at 785 nm and 1550 nm in fog and haze for optical wireless communications, in: Optical Wireless Communications III, vol. 4214, International Society for Optics and Photonics, 2001, pp. 26–37.

[39] A.G. Alkholidi, K.S. Altowij, Free space optical communications—theory and practices, in: Contemporary Issues in Wireless Communications, 2014, pp. 159–212.

[40] H. Ghazzai, E. Yaacoub, M. Alouini, Z. Dawy, A. Abu-Dayya, Optimized LTE cell planning with varying spatial and temporal user densities, IEEE Trans. Veh. Technol. 65 (3) (2016) 1575–1589.
[41] W. Shi, J. Li, W. Xu, H. Zhou, N. Zhang, S. Zhang, X. Shen, Multiple drone-cell deployment analyses and optimization in drone assisted radio access networks, IEEE Access 6 (2018) 12 518–12 529.
[42] J. Cho, J. Kim, Performance comparison of heuristic algorithms for uav deployment with low power consumption, in: 2018 International Conference on Information and Communication Technology Convergence (ICTC), 2018, pp. 1067–1069.
[43] J.M. Kahn, J.R. Barry, Wireless infrared communications, Proc. IEEE 85 (2) (1997) 265–298.
[44] Thorlabs, Thorlabs NIR bandpass and laser line filters: 700–1650 nm center wavelength, (online), available: https://www.thorlabs.com/newgrouppage9.cfm?objectgroup_id=1000, 2018.
[45] M. Kinoshita, T. Yamazato, H. Okada, T. Fujii, S. Arai, T. Yendo, K. Kamakura, Modeling and parameter estimation of vehicle vibration inducing transmitter displacement in ITS image sensor communication, in: 2017 IEEE International Conference on Communications Workshops (ICC Workshops), IEEE, 2017, pp. 144–149.
[46] P. Harikrishnan, V.P. Gopi, Vehicle vibration signal processing for road surface monitoring, IEEE Sens. J. 17 (16) (2017) 5192–5197.
[47] Y. Kaymak, R. Rojas-Cessa, J. Feng, N. Ansari, M. Zhou, On divergence-angle efficiency of a laser beam in free-space optical communications for high-speed trains, IEEE Trans. Veh. Technol. 66 (9) (2017) 7677–7687.
[48] J. Ma, G. Lu, L. Tan, S. Yu, Y. Fu, F. Li, Satellite platform vibration influence on acquisition system for intersatellite optical communications, Opt. Laser Technol. 138 (2021) 106874.